

## Article

# Crystal Structure of Aspartate Semialdehyde Dehydrogenase from *Porphyromonas gingivalis*

Jisub Hwang<sup>1,2,†</sup>, Hackwon Do<sup>1,2,†</sup>, Youn-Soo Shim<sup>3,\*</sup> and Jun Hyuck Lee<sup>1,2,\*</sup>

<sup>1</sup> Research Unit of Cryogenic Novel Material, Korea Polar Research Institute, Incheon 21990, Republic of Korea; hjsub9696@kopri.re.kr (J.H.); hackwondo@kopri.re.kr (H.D.)

<sup>2</sup> Department of Polar Sciences, University of Science and Technology, Incheon 21990, Republic of Korea

<sup>3</sup> Department of Dental Hygiene, Sunmoon University, Asan 31460, Republic of Korea

\* Correspondence: shim-21@hanmail.net (Y.-S.S.); junhyucklee@kopri.re.kr (J.H.L.);

Tel.: +82-41-530-2740 (Y.-S.S.); +82-32-760-5555 (J.H.L.); Fax: +82-41-530-2726 (Y.-S.S.); +82-32-760-5509 (J.H.L.)

† These authors contributed equally to this work.

**Abstract:** Aspartate semialdehyde dehydrogenase (ASADH) catalyzes the biosynthesis of several essential amino acids, including lysine, methionine, and threonine, and bacterial cell components. Thus, ASADH is a crucial target for developing new antimicrobial agents that can potentially disrupt the biosynthesis of essential amino acids, thereby inhibiting the growth of pathogens. Herein, the crystal structures of ASADH obtained from *Porphyromonas gingivalis* (PgASADH, UniProtKB code A0A1R4DY25) were determined in apo- and adenosine-2'-5'-diphosphate (2',5'-ADP)-bound complex forms at a resolution of 1.73 Å. The apo- and 2',5'-ADP-complexed crystals of PgASADH belonged to the space groups of  $I2_12_12_1$  and  $C222_1$ , respectively. Analytical size-exclusion chromatography showed a stable PgASADH dimer in a solution. Clustering analysis and structural comparison studies performed on PgASADH and previously known ASADHs revealed that ASADHs, including PgASADH, can be classified into three types depending on sequential and structural differences at the  $\alpha$ -helical subdomain region. These findings provide valuable insights into developing structure-based species-specific new antibacterial drugs against the oral pathogen *P. gingivalis*.

**Keywords:** crystal structure; oral pathogen; PgASADH; X-ray crystallography



check for updates

**Citation:** Hwang, J.; Do, H.; Shim, Y.-S.; Lee, J.H. Crystal Structure of Aspartate Semialdehyde Dehydrogenase from *Porphyromonas gingivalis*. *Crystals* **2023**, *13*, 1274. <https://doi.org/10.3390/cryst13081274>

Academic Editors: Bo Liang and Houfu Guo

Received: 31 July 2023

Revised: 14 August 2023

Accepted: 15 August 2023

Published: 18 August 2023



**Copyright:** © 2023 by the authors. Licensee MDPI, Basel, Switzerland. This article is an open access article distributed under the terms and conditions of the Creative Commons Attribution (CC BY) license (<https://creativecommons.org/licenses/by/4.0/>).

## 1. Introduction

*Porphyromonas gingivalis* (*P. gingivalis*) is a well-known periodontopathic pathogen associated with oral inflammation and periodontitis. Recently, *P. gingivalis* was identified as a risk factor for Alzheimer's disease, heart disease, diabetes, and rheumatoid arthritis, in addition to periodontitis [1]. Moreover, *P. gingivalis* was isolated from brain samples of patients with Alzheimer's disease [2] and its hazard potential with respect to neurological disorders was examined [3]. Therefore, discovering and developing therapeutic drugs are indispensable for patients infected with *P. gingivalis* to prevent periodontitis and further neurological disorders.

Aspartate semialdehyde dehydrogenase (EC 1.2.1.11; ASADH) is a nicotinamide adenine dinucleotide phosphate (NADP)-dependent enzyme and plays a key role in reductive dephosphorylation on aspartyl- $\beta$ -phosphate to produce aspartate  $\beta$ -semialdehyde (ASA). The product, ASA, is further processed into methionine, threonine, isoleucine, diaminopimelate (DAP), or lysine, which is vital for cell survival [4]. Notably, DAP serves as a cross-linking agent in bacterial cell-wall formation [4–6]. ASADH is promising as an antimicrobial drug target against infectious diseases for the following reasons: (1) Major targets of antibiotics are vital biological processes for cell survival, such as DNA, protein, and cell wall synthesis. In particular, ASADH-family enzymes are considered essential biocatalysts in redox and amino acid biosynthesis pathways. Gene knockout experiments have proved that *asd* null mutants are fatal to microorganism survival [7–9]. Since the

necessity of drug development for *P. gingivalis* is evident and ASADH is an excellent target biomolecule for antimicrobial compounds, structure-based research of ASADHs is a prerequisite for drug development for oral infections. (2) The majority of ASADHs have been discovered in bacteria and not in human and animal cells; thus, these enzymes can be valuable targets for developing antimicrobial agents. Furthermore, this approach can prevent adverse effects on the human body by avoiding non-specific drug binding. Consequently, a comprehensive biochemical and structural investigation of ASADH-family enzymes is necessary to meet the demand of the pharmaceutical industry from a public health perspective.

To date, several ASADHs derived from pathogenic microorganisms, including bacteria and fungi, have been biochemically and structurally characterized. They share highly conserved catalytic cysteine residues at the active site and acid/base catalyst histidine residues. The structural conformation of ASADH from *Escherichia coli* (PDB codes: 1BRM, 1T4B, 1T4D, and 1GL3) changes when it binds to an NADP cofactor and a reaction intermediate compound, and it may exhibit half-site reactivity [10–12]. Furthermore, two isoforms of ASADH obtained from *Vibrio cholera* (*VcASADH1* and 2) were discovered, and they shared only 27% sequence identity, showing a sequential and structural discrepancy on the  $\alpha$ -helical subdomain region at the interface (D183 to S224 of *VcASADH1*; 1MC4, N182 to C199 of *VcASADH2*; 2QZ9) [13,14]. These two isoforms of *VcASADH* showed that ASADHs might be classified into two types according to the difference in local sequence and structural moiety.

In the present study, the ASADH-encoding gene of *P. gingivalis* was cloned to obtain the target protein *PgASADH* for drug development. Comparative sequence alignment and structural studies of *PgASADH* and other previously known ASADH homolog structures were performed to understand the differences in structural conformations and active site residue configurations. Collectively, these findings provide better insights into designing an effective inhibitor to develop new specific drugs against *PgASADH*.

## 2. Materials and Methods

### 2.1. Plasmid Construction and Protein Expression and Purification

*PgASADH* (UniProt code: A0A1R4DY25; residues 1–337) was discovered in the *P. gingivalis* ATCC 33277 genome (Refseq: NC\_010729.1), and the gene was synthesized and cloned into the pET28a vector using *NdeI* and *XhoI* restriction enzymes. The recombinant plasmid was transformed into *Escherichia coli* BL21 (DE3) for expression. For *PgASADH* expression, a seed culture was inoculated into 3 L of Luria–Bertani broth containing 50  $\mu$ g/mL kanamycin, and the culture was incubated at 37 °C. Isopropyl  $\beta$ -D-1-thiogalactopyranoside (1 mM) was added when the optical density at 600 nm reached 0.5 for inducing *PgASADH* overexpression. The cells were cultured overnight at 25 °C and collected via centrifugation at 2800  $\times$  g for 20 min. The cell pellet was resuspended in a lysis buffer (20 mM Tris-HCl, pH 8.0, 200 mM NaCl, 5 mM imidazole) and sonication was performed to disrupt the cell wall and membrane. The cell debris was removed via centrifugation at 28,600  $\times$  g for 50 min and the supernatant was loaded onto a pre-equilibrated Ni-NTA column. The flow-through was discarded and the *PgASADH*-bound column was washed with a wash buffer (20 mM Tris-HCl, pH 8.0, 200 mM NaCl, 30 mM imidazole). *PgASADH* was eluted with a high concentration of an imidazole buffer (20 mM Tris-HCl, pH 8.0, 200 mM NaCl, 300 mM imidazole). Polyhistidine-tag (6X-His) at the N-terminal of *PgASADH* was then cleaved by incubating it with thrombin protease overnight at 4 °C. Finally, size-exclusion chromatography (SEC) was performed to obtain highly purified *PgASADH*, which was then transferred to a protein storage buffer (20 mM Tris-HCl, pH 8.0, 200 mM NaCl). The purity of *PgASADH* was evaluated using sodium dodecyl sulfate–polyacrylamide gel electrophoresis (SDS-PAGE). The purified *PgASADH* was concentrated at 20 mg/mL and stored at –80 °C.

## 2.2. Crystallization and Data Collection of Apo and Complex Forms

Crystallization conditions were monitored using an automatic liquid handler (Mosquito; TTP labtech, Hertfordshire, UK) as mentioned in the sitting-drop vapor diffusion method. Commercially available screening kits (MCSG I–IV, Index; Anatrace, OH, USA, and PGA screen, Morpheus; Molecular Dimensions, Rotherham, UK) were used for initial crystallization screening. The apo-complexed protein solution was mixed with each reservoir solution in a 1:1 ratio and every single droplet was equilibrated against 70  $\mu$ L of the reservoir solution. The cofactor-bound complex crystals were obtained via a co-crystallization method using NADP as a cofactor. The protein and ligand were mixed in a 1:6 molar ratio and incubated for 30 min at 25 °C before mixing with the screening solution. After incubation for 2 days at 23 °C, the apo-complexed crystals of PgASADH were obtained using 0.2 M calcium acetate hydrate, 0.1 M MES: NaOH (pH 6), and 10% (*w/v*) isopropanol (MCSG II, G4), whereas NADP-complexed crystals were obtained using 0.2 M ammonium sulfate, 0.1 M HEPES (pH 7.5), and 25% (*w/v*) polyethylene glycol 3350 (Index, F8). The apo- and cofactor-complexed crystals were directly subjected to X-ray diffraction. For cryo-protection, the apo crystals were soaked into perfluoropolyether cryo oil, whereas the NADP-complexed crystals were transferred to 10% glycerol mixed with the reservoir solution. These cryo-protected crystals were then moved to a goniometer head at a synchrotron (PAL, Pohang, Republic of Korea). Diffraction data for both the apo- and NADP-complexed crystals of PgASADH were collected under  $-178$  °C and a total of 360 images were obtained using the 1° oscillation range per image. The data were indexed, integrated, and scaled using the XDS software (<https://xds.mr.mpg.de/>, accessed on 31 July 2023) [15].

## 2.3. Structure Determination and Refinement of the Apo- and Cofactor-Complexed Structures

The initial phasing problem in the CCP4 suite was solved using the molecular replacement method [16]. The apo PgASADH structure was determined using a template structure from the AlphaFold structure database (model number: AF-A0A1R4DY25-F1) [17] and then the obtained apo structure was used as a template to determine the NADP-complexed PgASADH structure. Manual model refinement was performed using Coot (<https://www2.mrc-lmb.cam.ac.uk/personal/pemsley/cool/>, accessed on 31 July 2023) [18], whereas automatic refinement was performed using Refmac5 (<https://www.ccp4.ac.uk/html/refmac5.html>, accessed on 31 July 2023) [19] and phenix.refinement (<https://phenix-online.org/documentation/reference/refinement.html>, accessed on 31 July 2023) [20]. Despite the iterative refinement of the NADP-complexed structure of PgASADH, the electron density on the nicotinamide moiety of NADP was barely interpretable. Thus, we modified the complex structure with 2',5'-ADP as a ligand. The final apo- and cofactor-complexed structures were validated using Molprobit (<https://www.ncbi.nlm.nih.gov/pmc/articles/PMC2803126/>, accessed on 31 July 2023) [21] and deposited in the protein data bank with appropriate accession numbers. (PDB code for apo: 8JUO; 2',5'-ADP complex: 8JUS). Data collection and refinement statistics are summarized in Table 1.

## 2.4. Analytical SEC

The oligomeric state of PgASADH in the solution was examined with analytical SEC using a Superdex 200 10/100 GL column (Cytiva, MA, USA). A standard protein mixture, which contained bovine thyroglobulin (670 kDa), g-globulins from bovine blood (150 kDa), albumin chicken egg grade VI (44.3 kDa), and ribonuclease A type I-A from bovine pancreas (15 kDa), was used to plot a correlation graph. PgASADH was eluted at a flow rate of 0.5 mL/min using a protein storage buffer (20 mM Tris-HCl, pH 8.0, 200 mM NaCl). The correlation equation for the standard protein mixture and PgASADH molecular weight were calculated and visualized using the Prism v5 software.

**Table 1.** X-ray diffraction data collection and refinement statistics.

Data Set	<i>PgASADH</i>	2',5'-ADP-Bound <i>PgASADH</i>
X-ray source	BL-5C (PAL)	BL-5C (PAL)
Space group	$I2_12_12_1$	$C222_1$
Unit-cell parameters (Å, °)	a = 74.86, b = 108.86, c = 162.07 $\alpha = \beta = \gamma = 90$	a = 74.99, b = 108.22, c = 160.4 $\alpha = \beta = \gamma = 90$
Wavelength (Å)	0.9796	0.9796
Resolution (Å)	29.75–1.73 (1.79–1.73)	28.46–1.73 (1.79–1.73)
Total reflections	920,322 (91,009)	929,371 (90,382)
Unique reflections	69,004 (6845)	68,236 (6742)
Average I/σ (I)	19.59 (2.03)	29.89 (7.46)
$R_{\text{merge}}^a$	0.073 (1.269)	0.060 (0.306)
Redundancy	13.3 (13.3)	13.6 (13.4)
Completeness (%)	99.5 (99.9)	100 (100)
Refinement		
Resolution range (Å)	29.75–1.73 (1.75–1.73)	28.46–1.73 (1.79–1.73)
No. of reflections of the working set	68,955 (6841)	68,224 (6742)
No. of reflections of the test set	3363 (310)	3412 (337)
No. of amino acid residues	670	670
No. of water molecules	346	419
$R_{\text{cryst}}^b$	0.217 (0.321)	0.184 (0.204)
$R_{\text{free}}^c$	0.238 (0.333)	0.206 (0.244)
R.m.s. bond length (Å)	0.008	0.009
R.m.s. bond angle (°)	0.95	1.01
Average B value (Å <sup>2</sup> ) (protein)	28.25	17.84
Average B value (Å <sup>2</sup> ) (solvent)	28.30	25.14
Average B value (Å <sup>2</sup> ) (ligand)	-	24.09

<sup>a</sup>  $R_{\text{merge}} = \sum |<I> - I| / \sum <I>$ . <sup>b</sup>  $R_{\text{cryst}} = \sum ||F_o| - |F_c|| / \sum |F_o|$ . <sup>c</sup>  $R_{\text{free}}$  calculated with 5% of all reflections excluded from refinement stages using high-resolution data. Values in parentheses refer to the highest-resolution shells.

### 2.5. Comparative Bioinformatics Analysis

Structurally homologous enzymes were searched using the Dali-lite server, and proteins with high structural similarity (Z score > 39) were selected for comparative analysis. Structural superposition and multiple sequence alignment were performed using PyMOL v4.6 and ClustalX v2.1, respectively. The sequence similarity-based clustering analysis of ASADH homologous enzymes was performed based on the sequences in the UniProt database using CLANS, a clustering and visualization software in MPI Bioinformatics Toolkit [22]. A total of 100 full-length protein sequences were obtained using NCBI BlastP based on the pairwise score of the sequence against that of *PgASADH* and classified into four groups using CLANS. The interactions and *p*-values of highly scoring segment pairs between the two proteins were represented with nodes and edges, respectively. The *p*-value threshold ( $1 \times 10^{-4}$ ) was used in this study. Additionally, multiple-sequence alignment was performed and visualized using ClustalX v2.1 and GeneDoc v2.7, respectively. Using the same dataset, the residue-specific conservation score was determined and visualized using the Web-based ConSurf software [23]. The evolutionary amino acid conservation scores were calculated with the Bayesian method and represented using the *PgASADH* structure based on a color gradient according to protein sequence alignment.

## 3. Results and Discussion

### 3.1. Apo Structure of *PgASADH*

With the help of crystallization and X-ray diffraction, the structure of the apo form of *PgASADH* was successfully determined at a resolution of 1.73 Å, and it belonged to the  $I2_12_12_1$  space group (Figure 1A,B). The two monomers found in an asymmetric unit were examined using the Matthews correlation coefficient method [24]; the Matthews coefficient was 2.22 and the solvent percentage was 44.5%. The apo-*PgASADH* structure was evaluated with the molecular replacement method using a sequence-based modeled template from the AlphaFold database (model number: AF-A0A1R4DY25-F1) and the structural refinement results showed 21.7% of  $R_{\text{factor}}$  and 23.8% of  $R_{\text{free}}$ . The structure contained

11  $\alpha$ -helices and 13  $\beta$ -strands in the monomer unit, and the  $\beta$ -strands comprised extended  $\beta$ -sheets with hydrogen bonding (Figure 1C). A conserved  $\beta$ - $\alpha$ - $\beta$  motif was observed at the N-terminal domain and the  $\alpha$ -helical bundles surrounded the  $\beta$  sheets, exhibiting a typical Rossmann fold. This fold binds to nucleotide cofactors of enzymes, such as NAD/NADP or FAD [10,14]. The results showed that *Pg*ASADH comprised 338 amino acid residues with a molecular weight of 37.3 kDa; the size of the monomer structure was examined using SDS-PAGE (Figure 2A). The analytical SEC results showed that *Pg*ASADH was in the dimer state in the solution (Figure 2B). Interactions at the dimeric interface were analyzed using the *PDBePISA* (Protein Interactions, Surfaces, and Assemblies) server [25], which showed the main 32 hydrogen bonding interactions, 20 salt bridges, and 57 non-bonded structural interactions. Additionally, an analysis of the accessible surface area of the apo-*Pg*ASADH structure indicated that the buried surface area of the dimer was about 2727 Å<sup>2</sup>, which was 18.4% of the total accessible area. The dimeric structure of *Pg*ASADH was re-generated with the *PISA* interface analysis and symmetry search in *PyMoL* (Figure 2C). In the protomer structure of *Pg*ASADH, the  $\alpha$ 6 helix seemed to protrude toward the solvent area; however, it was a component of the dimeric interface with its  $\alpha$ 6 helix on its symmetric structure. The majority of oligomers of ASADHs in a solution have been studied as dimers; however, some ASADHs derived from fungi exist as tetramers (the dimer of a dimer) during enzymatic reactions [26,27]. A structural homolog search performed using the Dali-lite server [28] showed that *Pg*ASADH exhibited the highest structural similarity with ASADH II from *V. cholerae* with a Z-score of 49.8 and a root mean square deviation of 0.7 Å against 264 aligned C $\alpha$  atoms.

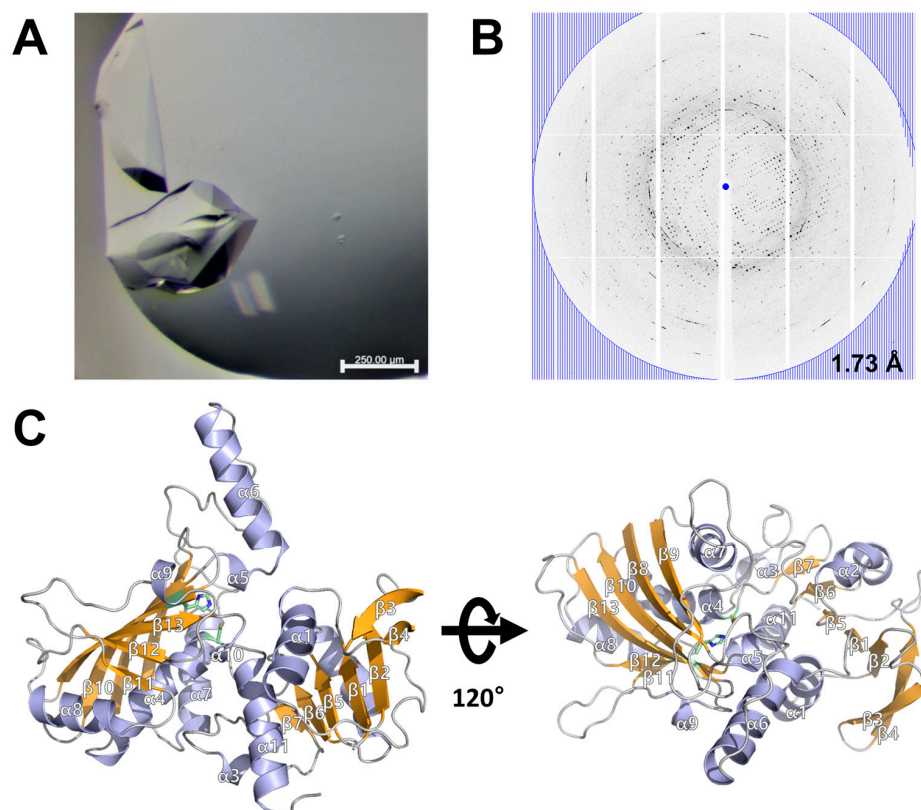


**Figure 1.** Crystallization, diffraction, and structure determination of aspartate-semialdehyde dehydrogenase obtained from *Porphyromonas gingivalis* (*Pg*ASADH). (A) Crystals of *Pg*ASADH in a 96-well sitting drop plate. The scale bar is shown at the bottom right. (B) X-ray diffraction results of *Pg*ASADH. The diffraction data were collected at a resolution of 1.73 Å. (C) The overall structure of *Pg*ASADH is shown as a ribbon diagram with 11  $\alpha$ -helices, shown in slate blue, and 13  $\beta$ -stands, shown in orange. Catalytic cysteine residue (C128) and acid/base catalyst histidine residue (H240) are shown as green sticks.

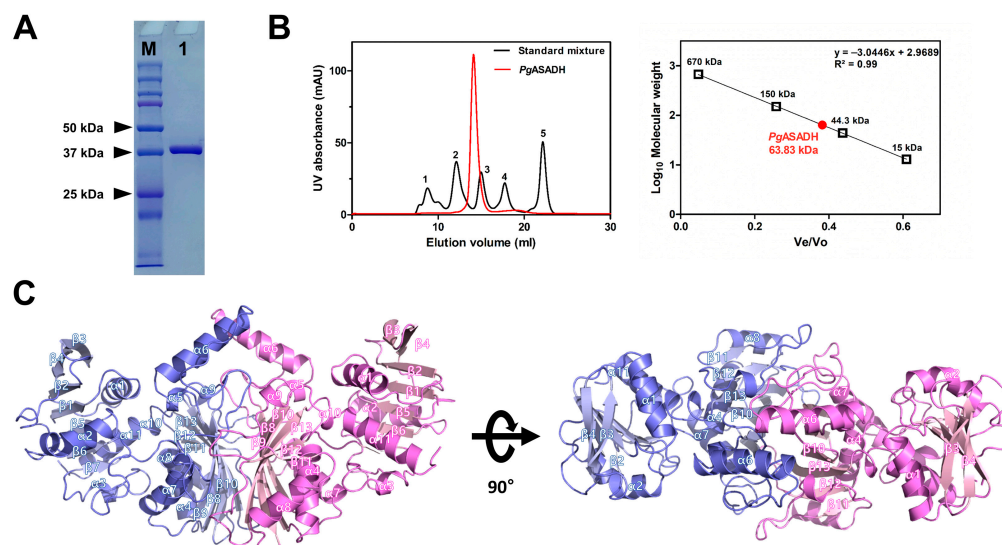


**Figure 2.** Dimerization of *PgASADH*. (A) Sodium dodecyl sulfate–polyacrylamide gel electrophoresis of *PgASADH*. (B) Analytical size-exclusion chromatography results showed the oligomeric state of *PgASADH* in the solution. 1: Bovine thyroglobulin (670 kDa), 2: g-globulins from bovine blood (150 kDa), 3: albumin chicken egg grade VI (44.3 kDa), 4: Ribonuclease A type I-A from bovine pancreas (15 kDa), 5: p-aminobenzoic acid (not shown in (B)). (C) Dimeric structure of *PgASADH* and its secondary structure. The asymmetric unit of ligand-free *PgASADH* crystal consists of two *PgASADH* molecules. The dimer structure is shown in two different colors (slate and light pink).

### 3.2. Cofactor-Bound Structure of *PgASADH*

The crystal structure of cofactor-bound *PgASADH* was determined at the same resolution (1.73 Å), showing that it belonged to the  $C222_1$  space group. Additionally, the cofactor-bound *PgASADH* structure was determined via the molecular replacement method using the refined apo-*PgASADH* structure as a template. The refinement results of the final structure showed an  $R_{\text{factor}}$  value of 18.4% and an  $R_{\text{free}}$  value of 20.6% for the cofactor-bound *PgASADH* structure. Similar to the apo-form of *PgASADH*, in the asymmetric unit, the complex structure contained two monomers. The *PgASADH* structure contained binding pockets for the substrate aspartate-semialdehyde and co-factor NADP. Initially, we constructed the NADP-complexed crystal of *PgASADH* to investigate the NADP binding mode. The structure refinement results showed that only the electron density map of the 2',5'-ADP region was visible; thus, the 2',5'-ADP model fitted into the electron density map. The nicotinamide ring in NADP was completely disordered and showed no electron density map. Hence, we determined the 2',5'-ADP-bound *PgASADH* structure, although NADP was initially added for complex crystallization (Figure 3). Previously, 2',5'-ADP was used as an NADP analog in crystallization experiments to investigate the cofactor binding mode for ASADH enzymes [29,30]. The structural comparison between the apo- and 2',5'-ADP-bound *PgASADH* protomer structures highlighted local conformational changes. Specifically, the  $\beta 2$ - $\beta 3$  and  $\beta 4$ - $\beta 5$  loop regions and  $\alpha 2$  and  $\alpha 7$ -helix regions showed a slight conformational movement toward 2',5'-ADP (Figure 4). The cofactor binding mode probably did not induce significant conformational changes in the overall structure or even in the active site of *PgASADH*.

### 3.3. Active Site of *PgASADH*

The sequence-based domain prediction (InterProScan) showed that the *PgASADH* structure comprised two different cofactor- (residues 2–118) and substrate (residues 137–316)-binding domains. In the 2',5'-ADP-bound structure, the cofactor binding domain and ligand closely interacted through several hydrophobic (Gly7, Val8, Gly10, Gly34, Leu55, Ala71, and Phe79) and hydrogen bonds with the OG atom of Ser9, Ser35, and Ser38

and the NH1 atom of Arg37. The structural superposition of apo-*Pg*ASADH and 2',5'-ADP-bound *Pg*ASADH revealed that overall structures were similar; however, the movements of several side chains of residues that interacted with 2',5'-ADP (Ser9, Ser35, Arg37, and Ser38) were observed. Both structures showed open conformation compared with the ternary-complexed (NADP and l-aspartate- $\beta$ -semialdehyde) structure of *Sp*ASADH (PDB code 2GZ3) (Figure 5A,B). Thus, 2',5'-ADP binding probably could not induce domain closing in *Pg*ASADH. The structural superposition of 2',5'-ADP-bound *Pg*ASADH and the ternary complex structure of *Sp*ASADH (PDB code 2GZ3) revealed that *Pg*ASADH contained different residues in the co-factor- and substrate-binding sites, compared with *Sp*ASADH. Specifically, the Thr11 residue interacted with the 2'-phosphate ion of NADP in *Sp*ASADH via a hydrogen bond, whereas *Pg*ASADH contained the Ser9 residue in the same position. In the *Sp*ASADH structure, the Asn325 residue formed a hydrogen bond with the O7N atom of the nicotinamide ring of the bound NADP. However, *Pg*ASADH contained the Gln313 residue in the same position, thereby blocking the binding site of the nicotinamide ring. Since the Gln residue has one more methylene group than Asn at the side chain, the drawback movement of Gln313 might be required for the tight binding of NADP in *Pg*ASADH (Figure 5C).

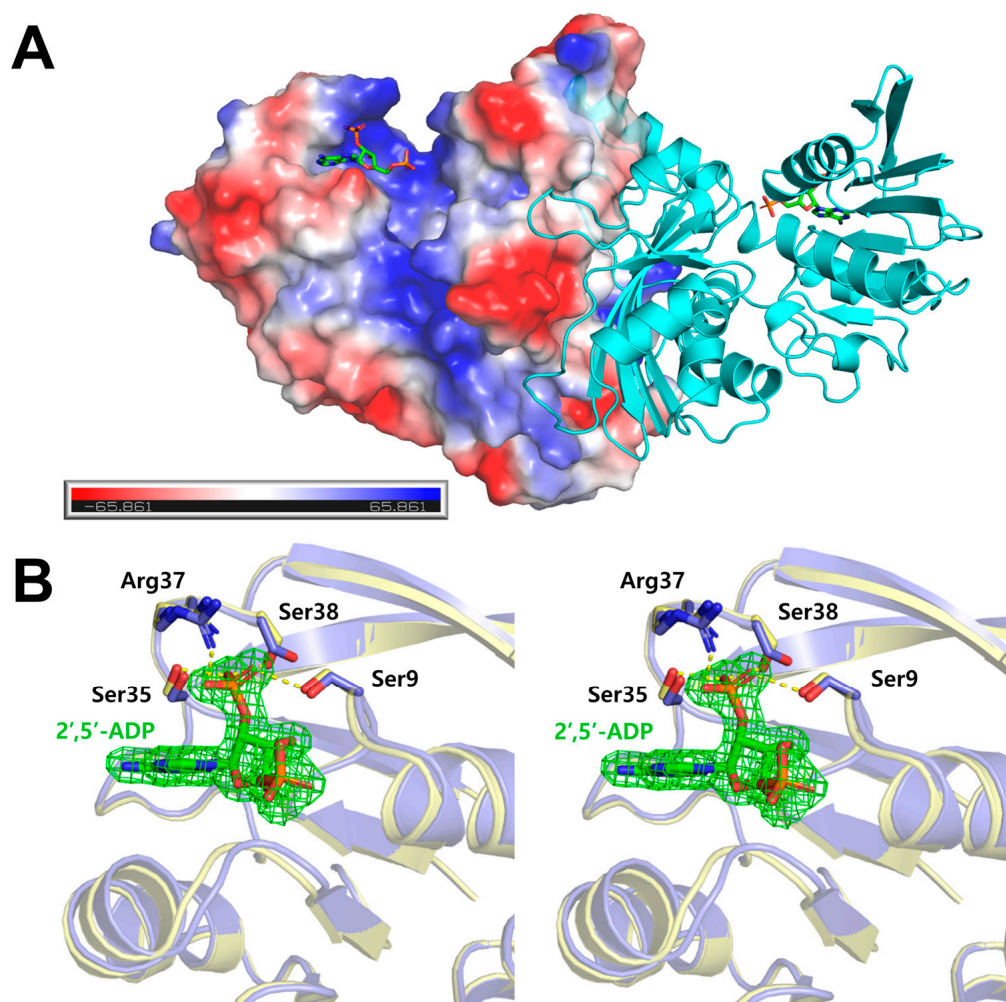


**Figure 3.** Adenosine-2',5'-diphosphate (2',5'-ADP)-bound *Pg*ASADH structure. (A) The overall 2',5'-ADP-bound structure of *Pg*ASADH is represented using electrostatic surface potential (chain A) and a cartoon (chain B, cyan) model. (B) Coenzyme binding sites of apo (slate)- and 2',5'-ADP (green)-bound complex structures (yellow) in stereo-view (cross-eye). The electron density map for 2',5'-ADP is presented in mesh (green) with a contour level of 1.0  $\delta$ .

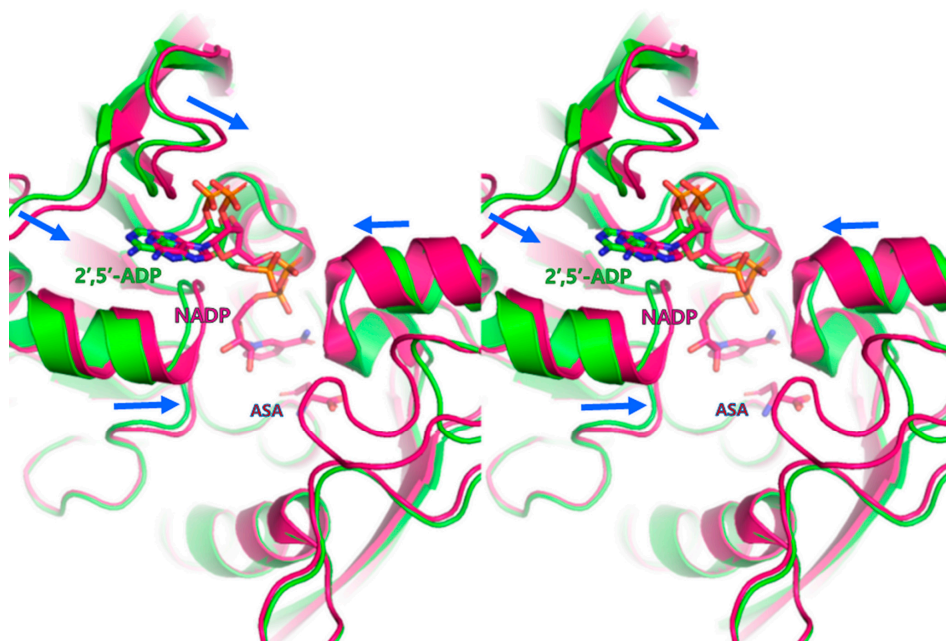


**Figure 4.** Superimposed structures of 2',5'-ADP-bound *PgASADH* with ternary-complexed *SpASADH* (PDB code 2GZ3). The 2',5'-ADP-bound structure of *PgASADH* (green) has open conformation, whereas the ternary-complexed *SpASADH* structure (magenta) has closed conformation. The conformational movement is represented by blue arrows.

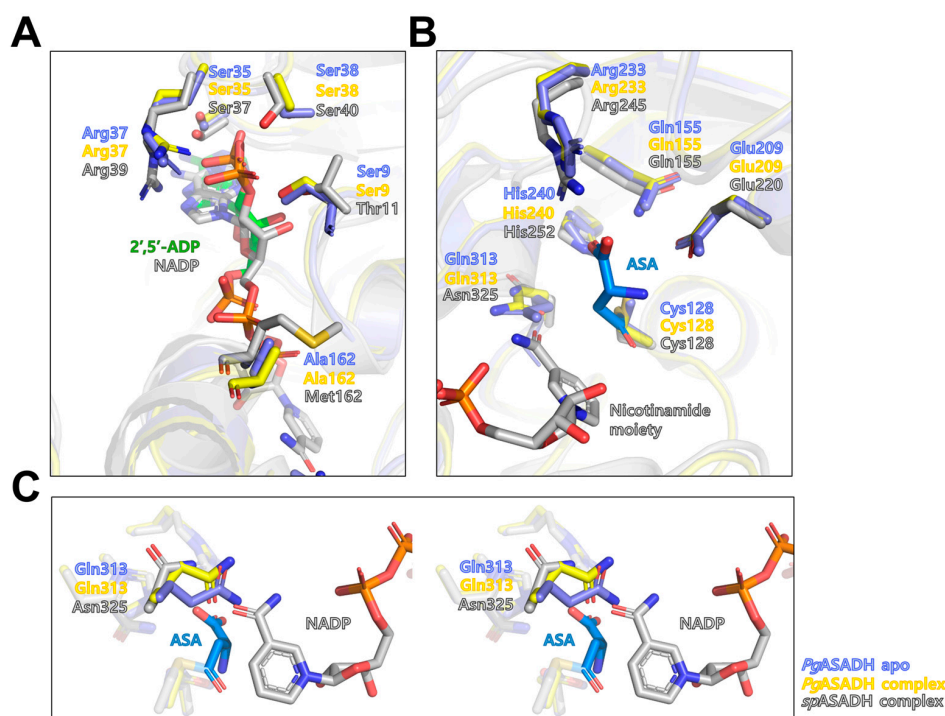


**Figure 5.** Structural comparison between *PgASADH* and *SpASADH*. Structural comparison of the coenzyme-binding site (A) and substrate-binding site (B) between apo- (slate) and 2',5'-ADP-bound (yellow) structures of *PgASADH* and NADP-bound *SpASADH* (light gray). 2',5'-ADP, NADP, and aspartate-semialdehyde (ASA) are colored green, light gray, and blue, respectively. (C) Stereo-view of the superposed nicotinamide binding moiety of the apo and complex structure of *PgASADH* and *SpASADH*.

### 3.4. Comparative Sequential and Structural Analysis of ASADHs

The multiple amino-acid sequence alignment of *Pg*ASADH and its structural homologs from the Dali search results (Table 2) showed that the enzymes might be categorized into two groups according to the sequence discrepancy in the  $\alpha 6$  helix– $\alpha 6$ – $\alpha 7$  loop region (Figure 6C). This sequence region corresponded to that in the  $\alpha 6$ – $\alpha 7$  loop in the tertiary structure of *Pg*ASADH. Furthermore, the ASADH homologs were apparently divided into type I and II based on differences that were observed by structural superposition (Figure 6A,B). The significant difference between the two types of ASADH was observed in the length of the  $\alpha 6$ – $\alpha 7$  loop region and the existing additional  $\alpha$ -helical secondary structure. In previous studies, two isoforms of ASADHs from *V. cholerae* [13,14] were categorized based on a local discrepancy between identical regions in the above-described sequence and structure. Herein, we compared type I and type II ASADHs, including two isoforms of *Vc*ASADHs (*Vc*ASADH1 and *Vc*ASADH2). Compared with type II-ASADHs, type I ASADHs contained extra sequences and an additional  $\alpha$  helix was observed in their structural regions. Specifically, type I ASADHs contained the  $\alpha$ -helical sub-domain at the dimerization interface, which probably affected its binding affinity during oligomerization.

**Table 2.** Structural homolog search result for *Pg*ASADH from a DALI search (the DALI-Lite server).

Protein	PDB Code	DALI Z-Score	UniProtKB Code	Sequence % ID with <i>Pg</i> ASADH (Aligned Residue Number)	Reference
ASADH from <i>Vibrio cholerae</i>	2QZ9	49.8	P23247	46 (330/336)	[14]
ASADH from <i>Thermus thermophilus</i> HB8	2YV3	47.8	Q5SKU8	46 (327/328)	Not yet published
ASADH from <i>Streptococcus pneumoniae</i> SP23-BS72	3PYL	47.7	<sup>a</sup> N/A	44 (333/362)	[29]
ASADH from <i>Mycobacterium tuberculosis</i> H37Rv	3VOS	47.6	P9WNX5	42 (324/343)	[31]
ASADH from <i>Pseudomonas aeruginosa</i> PAO1	2HJS	42.5	O87014	42.5 (328/334)	Not yet published
ASADH from <i>Francisella tularensis</i>	4WOJ	40.0	Q8G8T7	26 (329/365)	[32]
ASADH from <i>Acinetobacter baumannii</i>	7SKB	39.9	V5VGT0	27 (332/374)	Not yet published
ASADH from <i>Escherichia coli</i>	1GL3	39.4	P0A9Q9	27 (327/368)	[11]
ASADH from <i>Haemophilus influenzae</i> Rd KW20	1PQU	39.1	P44801	30 (328/372)	[33]

<sup>a</sup> N/A, sequence information is not available in the UniProtKB code database because this sequence was derived from metagenome information.

A total of 100 proteins were searched in the UniProtKB database using the *BlastP* function to investigate whether this classification could be applied to other *Pg*ASADH homologs [34] and used for clustering analysis by CLANS [22]. The clustering results showed that the enzymes were grouped into ASADH- and *N*-acetyl- $\gamma$ -glutamyl-phosphate reductase families (Figure 7A). Additionally, a total of 46 ASADH-family enzymes, including *Pg*ASADH, were subdivided into three subgroups depending on sequence similarity and phylogenetic analysis using the CLANS algorithm. Among these three subgroups of ASADHs, two groups showed highly similar sequential tendencies in the  $\alpha 6$  helix– $\alpha 6$ – $\alpha 7$  loop region (Figure S1). Thus, these two groups were referred to as type I and type II ASADHs. One additional subgroup of ASADHs observed in this clustering analysis was labeled as type III ASADHs.

Interestingly, type I ASADHs tightly adhered to pathogenic bacterium-derived ASADHs such as *E. coli* K-12 (UniProtKB code P0A9Q9), *V. cholera* O1 (UniProtKB code Q9KQG2), and *Pseudomonas aeruginosa* PAO1 (UniProtKB code Q51344). Type II ASADHs, including *Pg*ASADH, adhered to pathogenic and environmental bacterium-derived ASADHs together. Pathogenic bacteria such as *Campylobacter jejuni* (UniProtKB code Q59291) and *Helicobacter pylori* (UniProtKB code O25801) and environmental bacteria such as *Prochlorococcus marinus* (UniProtKB code P49420) were grouped into one cluster. The source organisms for Type III enzymes included archaea and fungi such as *Archaeoglobus fulgidus* (UniProtKB code O28766), *Methanocaldococcus jannaschii* (UniProtKB code Q57658), *Saccharomyces cerevisiae* (UniProtKB code P13663), *Schizosaccharomyces pombe* (UniProtKB code P78780), and one pathogenic bacterium, *Leptospira interrogans* (UniProt KB code P41394) (Table S1). Similarly, in multiple sequence alignment, these ASADHs were classified into three types. Furthermore, the evolutionary conservation score of residues between 46 ASADH homologs, including *Pg*ASADH, was mapped on the *Pg*ASADH monomer.

The dimerization interface area formed with  $\beta$ -strands was highly conserved; however, the  $\alpha$ -helical sub-domain (the  $\alpha 6$ - $\alpha 7$  loop region), which was involved in intermolecular interactions, showed a comparatively low conservation score (Figure 7B). The  $\alpha 6$  helix- $\alpha 6$ - $\alpha 7$  loop region of *Pg*ASADH showed marked differences, based on which ASADHs were divided into three types (Figure S1). Thus, this classification system can probably be applied to developing drug molecules to target specific species. Furthermore, this classification system may help physicians to efficiently prescribe specific drugs according to the pathogen type in the future. As more pathogen- and environmentally derived ASADHs are found, the accuracy of this clustering and classification system is thought to be higher.

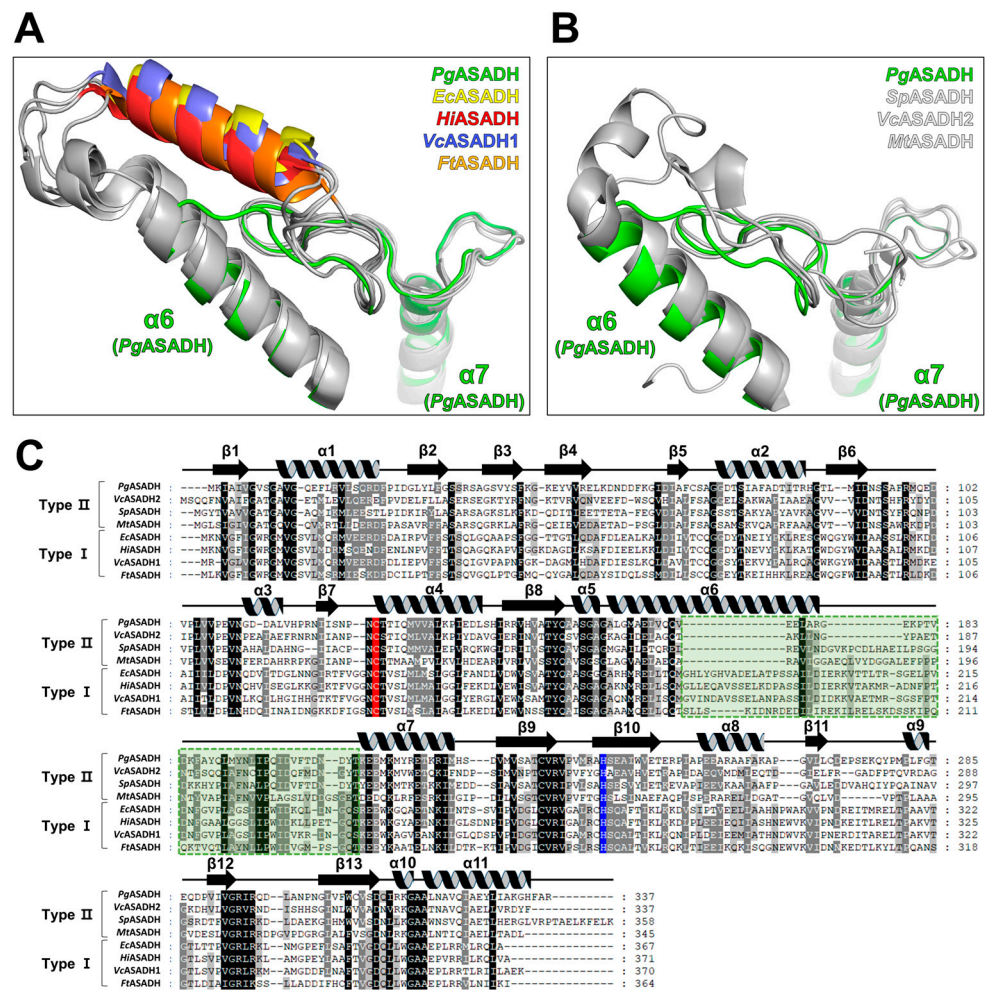


**Figure 6.** Structural superposition and multiple sequence alignment between *Pg*ASADH and homologous ASADH-family enzymes. Superposition of the  $\alpha 6$  region to the  $\alpha 7$  region of *Pg*ASADH with type I ASADHs (A) and type II ASADHs (B). (C) Multiple amino acid sequence alignments were performed between *Pg*ASADH (UniProtKB code A0A1R4DY25) and type I and type II ASADHs, including *Ec*ASADH from *Escherichia coli* (PDB codes 1BRM, 1T4B, 1T4D, and 1GL3; UniProtKB code P0A9Q9), *Hi*ASADH from *Haemophilus influenzae* (PDB codes 1NWC, 1NWH, 1TA4, 1TB4, 1NX6, 1OZA, 1PS8, 1PU2, 1Q2X, 1PQP, 1PR3, and 1PQU; UniProtKB code P44801), *Vc*ASADH type I from *Vibrio cholerae* (PDB codes 4R5M, 1MC4, 1MB4, 3Q0E, and 3PZR; UniProtKB code Q9KQG2), *Ft*ASADH from *Francisella tularensis* (PDB code 4WOJ; UniProtKB code Q8G8T7), *Vc*ASADH II from *Vibrio cholerae* (PDB codes 2R00 and 2QZ9; UniProtKB code P23247), *Sp*ASADH from *Streptococcus pneumoniae* (PDB codes 3Q1L and 4R3N; UniProtKB code Q8DQ00), and *Mt*ASADH from *Mycobacterium tuberculosis* (PDB codes 3VOS and 3TZ6; UniProtKB code P9WNX5). Conserved catalytic cysteine residue (C128) and acid/base catalyst histidine residue (H240) are indicated in red and blue, respectively. The  $\alpha$ -helical subdomain region is indicated with the green dotted box.

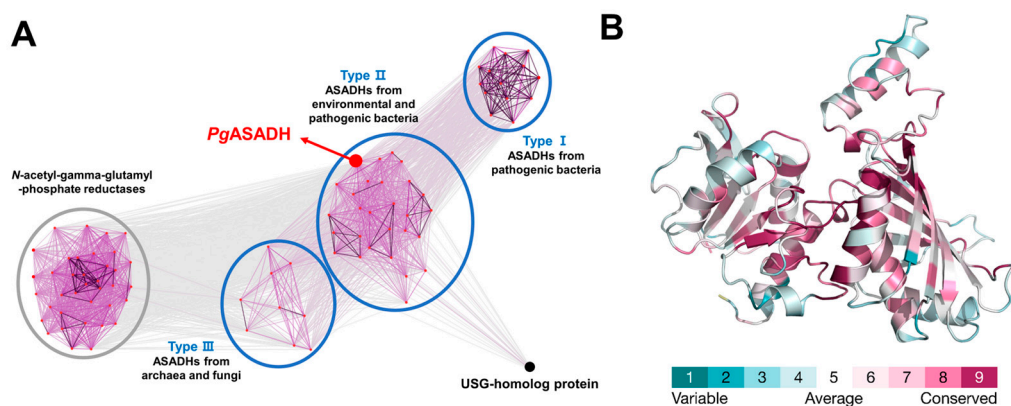


**Figure 7.** Sequence-based clustering and structural conservation score analysis of ASADH-family enzymes. (A) Clustering analysis for *PgASADH* and sequence-based similar enzymes using *CLANS*. Type I, II, and III ASADHs are marked by the blue circle, whereas *PgASADH* is indicated by the red dot and arrow. (B) The structural conservation score of residues was analyzed and mapped on the *PgASADH* structure using *Consurf*. The scale bar for the conservation score is mentioned below the structure.

In summary, the investigation of apo- and 2',5'-ADP-bound *PgASADH* structures implies coenzyme binding and the competitive inhibitory potential of 2',5'-ADP against ASADH enzymes. Comparative analysis using both sequential and structural approaches showed the potential of ASADH family proteins, which can be grouped by source organisms and pathogenicity. This comparative analysis reveals the importance of classifying ASADH-family proteins for drug development targeting infectious pathogens including *P. gingivalis*. The role of *PgASADH* in the survival and phenotype of oral pathogens should be studied further for practical drug development.

#### 4. Conclusions

In this study, the apo-complexed and 2',5'-ADP-bound crystal structures of *PgASADH* were determined. The 2',5'-ADP-complexed structure was considered weak to induce structural conformation into a closed form for enzyme reaction positioning. The local conformational changes were observed in the binding residues by structural superposition with other ASADH complex structures. The integrative analysis involving sequence-based clustering, structural superposition, and multiple sequence alignment showed that ASADHs can be classified according to discrepancies in the sequential and structural regions corresponding to the  $\alpha 6$ - $\alpha 7$  loop of *PgASADH*. The present study provides a basis for a structure-guided approach by determining the *PgASADH* crystal structure. Thus, further research on ASADH as a potential drug target for infectious diseases is crucial. Since ASADH is essential for cell survival, including for oral pathogens, the discovery of inhibitors for this enzyme implies drug development for the treatment of oral infectious disease.

**Supplementary Materials:** The following supporting information can be downloaded at: <https://www.mdpi.com/article/10.3390/cryst13081274/s1>, Figure S1: Multiple sequence alignment and classification of ASADHs. Table S1: Aspartate semialdehyde dehydrogenases used for clustering analysis.

**Author Contributions:** Conceptualization, Y.-S.S. and J.H.L.; Methodology, J.H. and H.D.; Validation, Y.-S.S. and J.H.L.; Resources, Y.-S.S. and J.H.L.; Writing—Original Draft Preparation, J.H., H.D., and Y.-S.S.; Writing—Review and Editing, Y.-S.S. and J.H.L.; Funding Acquisition, J.H.L. All authors have read and agreed to the published version of the manuscript.

**Funding:** This research was a part of the project titled “Development of potential antibiotic compounds using polar organism resources (KIMST 20200610, KOPRI Grant number PM23030)”, funded by the Ministry of Oceans and Fisheries, Republic of Korea.

**Acknowledgments:** We would like to thank the staff at the X-ray core facility of the Korea Basic Science Institute (KBSI; Ochang, Republic of Korea) and BL-5C of the Pohang Accelerator Laboratory (Pohang, Republic of Korea) for their assistance with data collection.

**Conflicts of Interest:** The authors declare no conflict of interest.

## References

1. Elwishahy, A.; Antia, K.; Bhusari, S.; Ilechukwu, N.C.; Horstick, O.; Winkler, V. *Porphyromonas gingivalis* as a risk factor to Alzheimer's disease: A systematic review. *J. Alzheimer's Dis. Rep.* **2021**, *5*, 721–732. [[CrossRef](#)] [[PubMed](#)]
2. Dominy, S.S.; Lynch, C.; Ermini, F.; Benedyk, M.; Marczyk, A.; Konradi, A.; Nguyen, M.; Haditsch, U.; Raha, D.; Griffin, C.; et al. *Porphyromonas gingivalis* in Alzheimer's disease brains: Evidence for disease causation and treatment with small-molecule inhibitors. *Sci. Adv.* **2019**, *5*, eaau3333. [[CrossRef](#)] [[PubMed](#)]
3. Ryder, M.I. *Porphyromonas gingivalis* and Alzheimer disease: Recent findings and potential therapies. *J. Periodontol.* **2020**, *91* (Suppl. 1), S45–S49. [[CrossRef](#)]
4. Viola, R.E. The central enzymes of the aspartate family of amino acid biosynthesis. *Acc. Chem. Res.* **2001**, *34*, 339–349. [[CrossRef](#)]
5. Paidhungat, M.; Setlow, B.; Driks, A.; Setlow, P. Characterization of spores of *Bacillus subtilis* which lack dipicolinic acid. *J. Bacteriol.* **2000**, *182*, 5505–5512. [[CrossRef](#)]
6. Pavelka, M.S., Jr.; Jacobs, W.R., Jr. Biosynthesis of diaminopimelate, the precursor of lysine and a component of peptidoglycan, is an essential function of *Mycobacterium smegmatis*. *J. Bacteriol.* **1996**, *178*, 6496–6507. [[CrossRef](#)]
7. Cardineau, G.A.; Curtiss, R., 3rd. Nucleotide sequence of the *asd* gene of *Streptococcus mutans*. Identification of the promoter region and evidence for attenuator-like sequences preceding the structural gene. *J. Biol. Chem.* **1987**, *262*, 3344–3353. [[CrossRef](#)] [[PubMed](#)]
8. Galan, J.E.; Nakayama, K.; Curtiss, R., 3rd. Cloning and characterization of the *asd* gene of *Salmonella typhimurium*: Use in stable maintenance of recombinant plasmids in *Salmonella* vaccine strains. *Gene* **1990**, *94*, 29–35. [[CrossRef](#)]
9. Harb, O.S.; Abu Kwaiq, Y. Identification of the aspartate-beta-semialdehyde dehydrogenase gene of *Legionella pneumophila* and characterization of a null mutant. *Infect. Immun.* **1998**, *66*, 1898–1903. [[CrossRef](#)]
10. Hadfield, A.; Kryger, G.; Ouyang, J.; Petsko, G.A.; Ringe, D.; Viola, R. Structure of aspartate-beta-semialdehyde dehydrogenase from *Escherichia coli*, a key enzyme in the aspartate family of amino acid biosynthesis. *J. Mol. Biol.* **1999**, *289*, 991–1002. [[CrossRef](#)]
11. Hadfield, A.; Shammass, C.; Kryger, G.; Ringe, D.; Petsko, G.A.; Ouyang, J.; Viola, R.E. Active site analysis of the potential antimicrobial target aspartate semialdehyde dehydrogenase. *Biochemistry* **2001**, *40*, 14475–14483. [[CrossRef](#)]
12. Nichols, C.E.; Dhaliwal, B.; Lockyer, M.; Hawkins, A.R.; Stammers, D.K. High-resolution structures reveal details of domain closure and “half-of-sites-reactivity” in *Escherichia coli* aspartate beta-semialdehyde dehydrogenase. *J. Mol. Biol.* **2004**, *341*, 797–806. [[CrossRef](#)]
13. Blanco, J.; Moore, R.A.; Kabaleeswaran, V.; Viola, R.E. A structural basis for the mechanism of aspartate-beta-semialdehyde dehydrogenase from *Vibrio cholerae*. *Protein Sci.* **2003**, *12*, 27–33. [[CrossRef](#)] [[PubMed](#)]
14. Viola, R.E.; Liu, X.; Ohren, J.F.; Faehnle, C.R. The structure of a redundant enzyme: A second isoform of aspartate beta-semialdehyde dehydrogenase in *Vibrio cholerae*. *Acta Crystallogr. D Biol. Crystallogr.* **2008**, *64*, 321–330. [[CrossRef](#)] [[PubMed](#)]
15. Kabsch, W. XDS. *Acta Crystallogr. D Biol. Crystallogr.* **2010**, *66*, 125–132. [[CrossRef](#)]
16. Winn, M.D.; Ballard, C.C.; Cowtan, K.D.; Dodson, E.J.; Emsley, P.; Evans, P.R.; Keegan, R.M.; Krissinel, E.B.; Leslie, A.G.; McCoy, A.; et al. Overview of the CCP4 suite and current developments. *Acta Crystallogr. D Biol. Crystallogr.* **2011**, *67*, 235–242. [[CrossRef](#)]
17. Jumper, J.; Evans, R.; Pritzel, A.; Green, T.; Figurnov, M.; Ronneberger, O.; Tunyasuvunakool, K.; Bates, R.; Ziřidek, A.; Potapenko, A.; et al. Highly accurate protein structure prediction with AlphaFold. *Nature* **2021**, *596*, 583–589. [[CrossRef](#)]
18. Emsley, P.; Cowtan, K. Coot: Model-building tools for molecular graphics. *Acta Crystallogr. D Biol. Crystallogr.* **2004**, *60*, 2126–2132. [[CrossRef](#)]
19. Murshudov, G.N.; Skubaák, P.; Lebedev, A.A.; Pannu, N.S.; Steiner, R.A.; Nicholls, R.A.; Winn, M.D.; Long, F.; Vagin, A.A. REFMAC5 for the refinement of macromolecular crystal structures. *Acta Crystallogr. D Biol. Crystallogr.* **2011**, *67*, 355–367. [[CrossRef](#)]
20. Afonine, P.V.; Grosse-Kunstleve, R.W.; Echols, N.; Headd, J.J.; Moriarty, N.W.; Mustyakimov, M.; Terwilliger, T.C.; Urzhumtsev, A.; Zwart, P.H.; Adams, P.D. Towards automated crystallographic structure refinement with phenix.refine.refine. *Acta Crystallogr. D Biol. Crystallogr.* **2012**, *68*, 352–367. [[CrossRef](#)]
21. Chen, V.B.; Arendall, W.B., 3rd.; Headd, J.J.; Keedy, D.A.; Immormino, R.M.; Kapral, G.J.; Murray, L.W.; Richardson, J.S.; Richardson, D.C. MolProbity: All-atom structure validation for macromolecular crystallography. *Acta Crystallogr. D Biol. Crystallogr.* **2010**, *66*, 12–21. [[CrossRef](#)]
22. Frickey, T.; Lupas, A. CLANS: A Java application for visualizing protein families based on pairwise similarity. *Bioinformatics* **2004**, *20*, 3702–3704. [[CrossRef](#)]
23. Yariv, B.; Yariv, E.; Kessel, A.; Masrati, G.; Chorin, A.B.; Martz, E.; Mayrose, I.; Pupko, T.; Ben-Tal, N. Using evolutionary data to make sense of macromolecules with a “face-lifted”. *ConSurf. Protein Sci.* **2023**, *32*, e4582. [[CrossRef](#)] [[PubMed](#)]
24. Matthews, B.W. Solvent content of protein crystals. *J. Mol. Biol.* **1968**, *33*, 491–497. [[CrossRef](#)]

25. Krissinel, E.; Henrick, K. Inference of macromolecular assemblies from crystalline state. *J. Mol. Biol.* **2007**, *372*, 774–797. [[CrossRef](#)] [[PubMed](#)]
26. Dahal, G.P.; Viola, R.E. Structure of a fungal form of aspartate-semialdehyde dehydrogenase from *Aspergillus fumigatus*. *Acta Crystallogr. F Struct. Biol. Commun.* **2017**, *73*, 36–44. [[CrossRef](#)]
27. Dahal, G.P.; Viola, R.E. Structural insights into inhibitor binding to a fungal ortholog of aspartate semialdehyde dehydrogenase. *Biochem. Biophys. Res. Commun.* **2018**, *503*, 2848–2854. [[CrossRef](#)] [[PubMed](#)]
28. Holm, L. Dali server: Structural unification of protein families. *Nucleic Acids Res.* **2022**, *50*, W210–W215. [[CrossRef](#)]
29. Pavlovsky, A.G.; Liu, X.; Faehnle, C.R.; Potente, N.; Viola, R.E. Structural characterization of inhibitors with selectivity against members of a homologous enzyme family. *Chem. Biol. Drug Des.* **2012**, *79*, 128–136. [[CrossRef](#)]
30. Pavlovsky, A.G.; Thangavelu, B.; Bhansali, P.; Viola, R.E. A cautionary tale of structure-guided inhibitor development against an essential enzyme in the aspartate-biosynthetic pathway. *Acta Crystallogr. D Biol. Crystallogr.* **2014**, *70*, 3244–3252. [[CrossRef](#)]
31. Vyas, R.; Tewari, R.; Weiss, M.S.; Karthikeyan, S. Structures of ternary complexes of aspartate-semialdehyde dehydrogenase (Rv3708c) from *Mycobacterium tuberculosis* H37Rv. *Acta Crystallogr. D Biol. Crystallogr.* **2012**, *68*, 671–679. [[CrossRef](#)] [[PubMed](#)]
32. Mank, N.J.; Pote, S.; Majorek, K.A.; Arnette, A.K.; Klapper, V.G.; Hurlburt, B.K.; Chruszcz, M. Structure of aspartate beta-semialdehyde dehydrogenase from *Francisella tularensis*. *Acta Crystallogr. F Struct. Biol. Commun.* **2018**, *74*, 14–22. [[CrossRef](#)] [[PubMed](#)]
33. Blanco, J.; Moore, R.A.; Faehnle, C.R.; Coe, D.M.; Viola, R.E. The role of substrate-binding groups in the mechanism of aspartate-beta-semialdehyde dehydrogenase. *Acta Crystallogr. D Biol. Crystallogr.* **2004**, *60*, 1388–1395. [[CrossRef](#)]
34. Johnson, M.; Zaretskaya, I.; Raytselis, Y.; Merezhuik, Y.; McGinnis, S.; Madden, T.L.; NCBI. NCBI BLAST: A better web interface. *Nucleic Acids Res.* **2008**, *36*, W5–W9. [[CrossRef](#)] [[PubMed](#)]

**Disclaimer/Publisher’s Note:** The statements, opinions and data contained in all publications are solely those of the individual author(s) and contributor(s) and not of MDPI and/or the editor(s). MDPI and/or the editor(s) disclaim responsibility for any injury to people or property resulting from any ideas, methods, instructions or products referred to in the content.